Flexible loops of New Delhi metallo-β-lactamase modulate its activity towards different substrates

Joanna E. Raczynska[a], Barbara Imiolczyk[a], Marlena Komorowska[a,b], Joanna Sliwiak[a], Justyna Czyrko-Horczak[c], Krzysztof Brzezinski[c*], Mariusz Jaskolski[a,b*]

[a]Center for Biocrystallographic Research, Institute of Bioorganic Chemistry, Polish Academy of Sciences, Poznan, Poland;

[b]Department of Crystallography, Faculty of Chemistry, A. Mickiewicz University, Poznan, Poland;

[3]Laboratory of Biochemistry and Structural Biology, Faculty of Chemistry, University of Bialystok, Poland

Corresponding authors: Krzysztof Brzezinski (k.brzezinski@uwb.edu.pl) and Mariusz Jaskolski (mariuszj@amu.edu.pl)

Article type: Research paper

Running head: Activity of NDM towards β-lactam substrates

For submission to: *International Journal of Biological Macromolecules*

Keywords: antibiotic resistance; NDM metallo-β-lactamase (MBL); crystal structure

Abbreviations: CENTA, yellow chromogenic cephalosporin; DTNB, 5,5'-dithiobis-(2-nitrobenzoic acid); HEPES, 4-(2-hydroxyethyl)-1-piperazineethanesulfonic acid; IPTG, isopropyl β-D-1-thiogalactopyranoside; MPD, 2-methyl-2,4-pentanediol; NDM, New Delhi metallo-β-lactamases; PEG, polyethylene glycol; TCEP, tris(2-carboxyethyl)phosphine; TEV, Tobacco Etch Virus; TNB, 2-nitro-5-thiobenzoic acid

Abstract

Two accessory loop regions that are present in numerous variants of New Delhi metallo-β-lactamases (NDM) are important for the enzymatic activity. The first one is a flexible loop L3 that is located near the active site and is thought to play an important role in the catalytic process. The second region, Ω loop is located close to a structural element that coordinates two essential zinc ions. Both loops are not involved in any specific interactions with a substrate. Herein, we investigated how the length and hydrophobicity of loop L3 influence the enzymatic activity of NDMs, by analyzing mutants of NDM-1 with various deletions/point mutations within the L3 loop. We also investigated NDM variants with sequence variations/artificial deletions within the Ω loop. For all these variants we determined kinetic parameters for the hydrolysis of ampicillin, imipenem, and a chromogenic cephalosporin (CENTA). None of the mutations in the L3 loop completely abolished the enzymatic activity of NDM-1. Our results suggest that various elements of the loop play different roles in the hydrolysis of different substrates and the flexibility of the loop seems necessary to fulfill the requirements imposed by various substrates. Deletions within the Ω loop usually enhanced the enzymatic activity, particularly for the hydrolysis of ampicillin and imipenem. However, the exact role of the Ω loop in the catalytic reaction remains unclear. In our kinetic tests, the NDM enzymes were inhibited in the β-lactamase reaction by the CENTA substrate. We also present the X-ray crystal structures of the NDM-1, NDM-9 and NDM-12 proteins.

1. Introduction

Discovered in 2008, New Delhi metallo-β-lactamase 1 (NDM-1) belongs to the B1 subgroup of metallo-β-lactamases (MBLs) [1]. Most B1 and B3 metallo-β-lactamases possess ~15-residue hairpin loop L3 near the active site (Figs. 1, 2A and 3A, B) that is thought to play an important role in the catalytic process [2, 3]. Metallo-β-lactamases of B1 subgroup have a similar length of this loop but different sequences (Fig. 2A), with the exception of Sao Paulo metallo-β-lactamase (SPM). SPM was reported to be a hybrid of B1/B2 subgroups because of its short L3 loop and an extended α3 region [4] (Fig. 2B). The enzymes belonging to the B1 and B3 subgroups of MBLs also share other structural similarities in the active site area. They usually bind two zinc ions in their active sites, that are required for their hydrolase function [5,6,7,8,9,10,11]. Moreover, one of these two Zn^{2+} coordination sites (referred to as the Zn1 site), composed of three His residues, is identical in these two subgroups of MBLs. On the other hand, the second zinc cation is coordinated in the Zn2 site by Asp-Cys-His or Asp-His-His triads in the B1 or B3 subgroups, respectively. The coordination spheres of the zinc ions located in active sites of B1 and B3 MBLs are completed by two water molecules.

The L3 loop of NDM-1 was found to be flexible [12] and it adopts different conformations in different NDM structures depending on its environment within the crystal. Fig. 3A shows five different arrangements of loop L3, all from a single PDB structure 3SPU of NDM-1 [13]. The structure contains five independent protein subunits and in each of them the loop adopts a different conformation and participates in different crystal contacts. Similar behavior is observed in the PDB structural model 6ACA, which is a mutant of NDM-1 containing an additional Pro residue in the L3 loop sequence [14] and where each of the four protein subunits shows a different conformation of loop L3 (Fig. 3B).

The L3 loop of NDM-1 is mostly hydrophobic but also contains a single charged Asp residue. Mutations within the loop or deletion of the entire loop region resulted in lower

activities of CcrA, IMP-1 and BcII metallo-β-lactamases [15,16,17]. However, no specific interactions of the loop with bound reaction product or inhibitor were reported so far based on existing crystal structures. In the structure 5ZGE with hydrolyzed ampicillin [18], the L3 loop does form hydrophobic interactions with the bound ligand (Fig. 3C), but the observed conformation of the loop is stabilized by extensive intermolecular interactions with another L3 loop, as well as the ligand, from a symmetry-related molecule in the crystal (Fig. 3D and E). The same behavior is also found in other structures of NDM-1 containing a hydrolyzed penicillin molecule: 4HL1, 4H0D, 4HL2 [19], 4EYF, 4EYB, 4EY2 [20], and 5O2F [21], which is a re-refinement of structure 4RL2, initially described as containing a hydrolyzed cephalosporin, cephalexin [22].

Spectroscopic studies of NDM-1 showed that the L3 loop closes down on the substrate during the catalytic reaction [23]. It was also found that changes in the sequence of the loop tune the reaction mechanism of NDM-1 by altering the protonation rate of an anionic reaction intermediate [14].

Currently, there are at least two dozen reported variants of New Delhi metallo-β-lactamase [24,25] usually differing from NDM-1 by one or two amino acid residues. Twelve of these variants have a substitution at position Met154, with the Met residue changed to Leu (most cases) or Val (NDM-11). This residue is located within a short loop connecting helix α3 and strand β8 (Fig. 1), according to the secondary structure numbering scheme presented by Zhang and Hao [26]. In this work, we will refer to this loop as the Ω loop. Another residue from this structural element, Glu152, is changed to Lys in NDM-9. The Ω loop lies in close proximity of loop L6, which contains three Zn^{2+}-binding ligands: His120, His122 and Asp124. However, there is no direct contact between the Ω loop residues and the reaction products in crystal structures of NDM-1 containing a product of antibiotic hydrolysis. Stewart

et al. [27] showed that variants NDM-4 and NDM-12, which harbor the M154L substitution, exhibit lower activity loss in conditions of low Zn^{2+} concentration compared to NDM-1, which helps to evade the host immune response. Substitution of Glu152 to Ala in NDM-5 resulted in a significant loss of activity [28].

In this work, we sought to investigate how the length of loop L3 and its hydrophobicity influence the enzymatic activity of New Delhi metallo-β-lactamases. Accordingly, we designed six artificial mutants of NDM-1 with deletions of up to six residues within this loop, as well as three artificial variants with point mutations that change the character of the loop to hydrophilic, either using uncharged or positively/negatively charged side chains (Fig. 2C). These variants are (acronyms in parentheses): NDM-ΔP68G69 (5ndm), NDM-ΔM67F70 (6ndm), NDM-ΔD66G71 (7ndm), NDM-ΔL65A72 (8ndm), NDM-ΔD66M67F70G71 (9ndm), NDM-ΔL65D66M67F70G71A72 (10ndm) and NDM-M67N-F70N (11ndm), NDM-D66N-M67E-F70E (12ndm), NDM-D66-M67K-F70K (13ndm). We also studied four natural variants: NDM-1, NDM-9 (E152K), NDM-11 (M154V) and NDM-12 (M154L/G222D), and two artificial mutants with deletions in the Ω loop: NDM-ΔQ151E152M154 (14ndm) and NDM-M154V-ΔQ151E152 (15ndm) (Fig. 2D). For all these variants we determined kinetic parameters for the hydrolysis of ampicillin, imipenem and the yellow chromogenic cephalosporin (CENTA). We also determined three X-ray crystal structures of the following variants: NDM-12 in complex with hydrolyzed ampicillin, NDM-9 with a phosphate ion bound in the active site, and a high-resolution structure of the reference enzyme NDM-1.

2. Materials and methods

2.1. Protein expression and purification

Gene sequences, cloned into pET-15b expression vector, were obtained from GenScript, initially by chemical synthesis and then mutagenesis. All sequences were codon-optimized

and coded residues 29-270, plus a His-tag at the N-terminus followed by a TEV protease cleavage site. The proteins were expressed in *E. coli* cells as follows. Cell cultures were grown at 37°C until reaching mid-log phase. Then, temperature was decreased to 18°C and 0.5 M isopropyl β-D-1-thiogalactopyranoside (IPTG) was added to induce protein expression, which continued for ~16 hours. Cells were pelleted by centrifugation at 6693 × *g* for 10 min, and the pellets were resuspended in a lysis buffer containing 50 mM HEPES·NaOH pH 8.0, 500 mM NaCl, 20 mM imidazole, 10% glycerol and 1.0 mM TCEP·HCl. For variants 5ndm, 6ndm, 7ndm, 8ndm, 9ndm, 10ndm, 14ndm, and 15ndm, the buffer additionally contained 2% sarkosyl. Cell lysis was performed by sonication and the soluble fraction was loaded on Ni-NTA column. After thorough washing, His-tagged TEV protease was applied onto the column to separate the recombinant protein from the column-bound His-tag and the reaction proceeded for three hours at room temperature with mixing to ensure proper contact between the two proteins. The proteins devoid of the His-tag were drained from the column and dialyzed into a buffer containing 50 mM HEPES·NaOH pH 7.0, 150 mM NaCl, 100 μM $ZnCl_2$ and 0.5 mM TCEP·HCl (for kinetic studies); or purified by gel filtration chromatography in 50 mM HEPES·NaOH pH 7.5, 150 mM NaCl, 100 μM $ZnCl_2$, 0.5 mM TCEP for crystallization. All proteins had similar expression yield of approximately 40 mg per 0.5 L of bacterial culture.

2.2. Crystallization

Proteins were concentrated to 40 mg/ml and used for robotic screening of crystallization conditions in 96-well plates using the sitting drop vapor diffusion method. For NDM-12, the protein solution contained additionally 30 mM ampicillin. The crystallization conditions were: 0.2 M CH_3COONH_4, 0.1 M Bis Tris pH 5.5, 25% w/v PEG 3350 (NDM-12); 0.2 M NaCl, 0.1 M phosphate/citrate buffer pH 4.2, 20% PEG 8000 (NDM-9); and 0.06 M $MgCl_2$,

0.06 M $CaCl_2$, 0.1 M imidazole·MES buffer system pH 6.5, 12.5% MPD, 12.5% PEG 1000, 12.5% PEG 3350 (NDM-1).

2.3. X-Ray data collection, structure solution and refinement

X-Ray diffraction data were measured at the BESSY synchrotron beamline 14.2 of the Helmholtz-Zentrum Berlin (6OL8) and at Petra III beamline P13, EMBL c/o DESY Hamburg (6OGO and 6TWT). The data were processed and scaled with *XDS* [29]. The observed intensities were converted to structure factor amplitudes using the program *Truncate* [30] from the *CCP4* package [31]. The phase problem was solved by molecular replacement with *Phaser* [32], using a single protein chain from the structure 5ZGE as a model. Structure refinement was performed in *Refmac* [33] and was interspersed with manual model rebuilding in *Coot* [34]. Structural figures were generated with *PyMOL* [35]. The structural models were validated with *MolProbity* [36] and the PDB validation server [37]. The final coordinates and structure factors were deposited in the Protein Data Bank [38] with accession codes 6OL8 (NDM-12), 6OGO (NDM-9) and 6TWT (NDM-1). The corresponding raw X-ray diffraction images were deposited in the RepOD Repository at the Interdisciplinary Centre for Mathematical and Computational Modelling (ICM) of the University of Warsaw, Poland, and are available for download with the following Digital Object Identifiers (DOI): http://dx.doi.org/10.18150/repod.3651042 (6OL8), http://dx.doi.org/10.18150/repod.7378742 (6OGO) and http://dx.doi.org/10.18150/repod.2797550 (6TWT).

2.4. Measurement of kinetic parameters

Kinetic data were obtained using a TECAN infinite®200 microplate reader. Reaction progress at 28°C was followed for 2 minutes by measuring absorption at 235 nm (ampicillin), 300 nm (imipenem) or 405 nm (CENTA). Initial reaction velocities were obtained from the

linear range of the progress curves using Δε values of -1050 cm^{-1} M^{-1} (ampicillin), -9393 cm^{-1} M^{-1} (imipenem) and 6400 cm^{-1} M^{-1} (CENTA). Three or four series were measured for each condition. Enzyme concentration was between 30-200 nM; the exact values for each reaction are given in Tables 1-3. Kinetic parameters for ampicillin and imipenem hydrolysis were fitted to the data with the program *GraFit* using the standard Michaelis-Menten kinetic model. For CENTA hydrolysis, we used a model with substrate inhibition, according to the formula:

$$V = \frac{V_{max}[S]}{K_M + \frac{[S]^2}{K_i} + [S]}$$

[1]

where K_M is the Michaelis constant, [S] is the initial substrate concentration, and K_i is the inhibition constant corresponding to inhibition by substrate. This model is also consistent with inhibition by reaction product, when product concentration is expressed as a function of the initial substrate concentration.

3. Results

3.1. Protein expression and activity

All proteins exhibited high expression yield in *E. coli* cultures, with the natural variants NDM-1, NDM-9, NDM-11, NDM-12 and mutants 11ndm, 12ndm, 13ndm present entirely in the soluble fraction after cell lysis. All the deletion mutants (5-10ndm) were mostly present in the insoluble fraction, from which they were extracted with the use of sarcosyl detergent as described in the Methods section. All protein solutions were pink-colored after elution from the Ni-NTA column. The color significantly faded after extensive dialysis to a buffer containing 100 μM of Zn^{2+} ions and was most likely caused by binding of Ni^{2+} ions from the

Ni-NTA column. Size exclusion chromatography performed for variants NDM-1, NDM-9, NDM-11 and NDM-12 and all the artificial mutants showed them to be monomeric in solution. All variants were active and hydrolyzed the chromogenic substrate CENTA which was used for initial activity tests.

3.2. Reaction kinetics

All of the NDM variants studied were active against the tested β-lactams (ampicillin, imipenem and CENTA). For ampicillin and imipenem, the hydrolysis reaction proceeded according to standard Michaelis-Menten kinetic mechanism, with K_M and k_{cat} as presented in Table 1 and Table 2. Variants 14ndm and 15ndm were considerably slower and higher enzyme concentration was used for reaction with these two substrates. For the natural variants, in the reaction with ampicillin, the K_M values determined by UV absorption measurements were within high micromolar range, which is higher than previously reported for this substrate [39,40]. Mutations in the L3 loop generally resulted in higher values of both K_M and k_{cat}, with the strongest effect observed for variants 8ndm, 10ndm and 13ndm (Table 1). On the other hand, deletions in the Ω loop resulted in decreased values of K_M and k_{cat} as compared to the wild-type enzymes, especially in the case of variant 15ndm, where this gives rise to higher catalytic efficiency. We observed a similar trend for imipenem hydrolysis (Table 2). For this substrate, K_M values for the natural variants were in the low micromolar range and the turnover rates were between ~70-140 s^{-1}. Here, the largest increase in the K_M value was observed for variants 5ndm, 8ndm, 9ndm, 10ndm and 13ndm. Variant 15ndm had a reduced K_M and k_{cat}, as for ampicillin, but 14ndm had K_M similar to that of the wild-type enzymes, although lower k_{cat}.

For the CENTA substrate, for most enzymes we observed decreased reaction rate at higher substrate concentrations (Fig. 4) and were not able to fit the standard Michaelis-Menten

kinetic reaction model into these data. Instead, we used a model with substrate/product inhibition as described in Methods. The natural variants NDM-1, NDM-9, NDM-11 and NDM-12 all exhibited moderate inhibition with K_i values (corresponding to substrate inhibition) of around 0.5 mM (Table 3) and K_M of around 1 mM. The weakest inhibition was observed for variants with deletions in loop L3: 8ndm, 9ndm and especially for 10ndm with no noticeable inhibition (fitted K_i=8.0 ± 6.5 mM for the latter variant). An exception to this trend is 6ndm with K_i of 0.5 mM and K_M > 2 mM. For 10ndm we were able to fit the standard kinetic model which gave rise to reasonable values of K_M and k_{cat} with small standard errors (Fig. 4C). At the other end of the spectrum, with strongest inhibition, are variants 15ndm with K_i=301 ± 135 μM and 13ndm with K_i=170 ± 69 μM (Fig. 4D).

3.3. Crystal structure of NDM-12 in complex with hydrolyzed ampicillin

The protein crystallized in $P2_12_12_1$ space group with two molecules in the asymmetric unit (ASU) and the same crystal packing as in other NDM-1 structures containing a hydrolyzed penicillin molecule, as described in the Introduction. The ligand is well defined in the electron density map and forms a hydrogen bond with the L3 loop from a symmetry-related molecule as in the PDB structure 5ZGE (Fig. 5A) and other structures of the enzyme crystallized in the presence of penicillin. The L3 loop has the same conformation and is engaged in the same crystal contacts as shown in Fig. 3D and E for 5ZGE. The loop conformation does not seem to be affected by the macromolecular environment. For example, Asp222 located in close proximity of the loop is well defined in the electron density and the G222D mutation (as compared to NDM-1) does not appear to influence the backbone conformation of loop L3 (Fig. 5A). Within both molecules in the asymmetric unit, two triads comprised of Glu152, Asp222 and Glu227 from a symmetry-related protein molecule are engaged in binding of metal cations which were modeled as sodium ions in the final model. It is possible, however,

that this binding site is partially occupied by a potassium cation, or that one of the two sites contains sodium and the other potassium ions. The resolution of the X-ray data is insufficient for a detailed analysis of this intermolecular metal binding site.

3.4. Crystal structure of NDM-9

The protein crystallized in $P3_1$ space group with three molecules in the asymmetric unit. A phosphate ion is bound at the active site, coordinating to Zn^{2+} and displacing the canonical Asp124 ligand (Fig. 6A and B). The phosphate ion also interacts with Arg45 from a symmetry-related protein molecule (Fig. 6B). There are also considerable differences in the conformation of other active-site residues as compared to our structure of NDM-12 and, after Cα alignment, the distance between the Zn^{2+} ions bound at the Zn2 site is 1.2 Å (Fig. 6C). The L3 loop has the same conformation in all three subunits with backbone conformation very similar to that observed in our structure of NDM-12 (Fig. 6D). However, the position of the Phe70 side chain is different with the phenyl ring forming hydrophobic interactions with a symmetry-related protein molecule and a PEG fragment bound at that interface. NDM-9 has an E152K mutation as compared to NDM-1. The side chain of Lys152 is visible in the electron density but not very well ordered. It forms a salt bridge with Asp223.

3.5. High-resolution crystal structure of NDM-1

Numerous attempts to obtain crystals of NDM-1 in complex with hydrolyzed CENTA have failed. On the other hand, very high quality crystals of NDM-1 were obtained in the presence of 1.0 mM 5,5'-dithiobis-(2-nitrobenzoic acid) (DTNB) and 1.5 mM of the reducing agent TCEP. The reduced form of DTNB, 2-nitro-5-thiobenzoic acid in its dideprotonated form (TNB^{2-}), corresponds exactly to the fragment that would be released from CENTA upon

its hydrolysis (Figs. 7A, B). However, no ligand was bound at the active site of the crystallized protein.

The space group of this crystal structure is the same as for NDM-12 ($P2_12_12_1$) but with different cell parameters and different crystal packing. Two molecules are present in the asymmetric unit and form an interface that is exactly the same as the interface between the two subunits in the NDM-12 structure (PDB ID: 6OL8). Superposition of chain A of NDM-12 on chain A of NDM-1 gives a Cα rmsd of 0.3 Å and also results in perfect alignment of the B chains. However, the symmetry-generated molecules in the two structures are rotated by 57° around the [010] direction (Fig. 5B). The conserved protein interface is supported by metal ion coordination *via* Glu152 and Asp223 (from molecule A or B) and Glu227 (from molecule B or A). These two metal sites are most likely occupied by calcium ions, as indicated by CBVS analysis [41] and the *CheckMyMetal* server [42]. Apart from metal-ion-mediated interactions, we also identified two pairs of hydrogen bonds supporting this intramolecular interface: His228_Nε2…Oε2_Glu152 and Gln147_Nε2…O_Tyr184.

4. Discussion

Two of the structures presented in this work (NDM-12 and NDM-1) share the same interface between two molecules in the ASU in spite of different crystal packing. This interface is also conserved in other structures of NDM-1 and its mutants: 3SPU (NDM-1) [13], 6CAC and 6C6I (NDM-1 mutants in the L3 loop) [14], and 5YPK (NDM-1) [43], each of these having different crystal packing. This suggests a biological role of this dimer interface, which was also noted by King and Strynadka [13]. In most of these structures the interface is supported by interactions with metal ions. In the native environment of bacterial periplasm this could allow these enzymes to bind additional Zn^{2+} ions, forming a metal cation reservoir for conditions of limited Zn^{2+} availability. One of the metal ligands is Glu152,

which in NDM-9 is replaced by Lys152. In physiological conditions, the lysine amino group is protonated and thus unable to coordinate a metal cation; not surprisingly, this interface is not conserved in the structure of NDM-9. It would be interesting to see whether there are any significant differences in the ability to withstand conditions of limited Zn^{2+} availability between NDM-9 and other NDM variants not harboring the E152K mutation. It is of note that residue E152 is part of the Ω loop, whose deletions did not affect the enzyme activity in our study. Moreover, kinetic parameters characterizing the enzymatic activity of the artificial mutants were usually significantly improved compared to the natural NDM-1 variant, as observed for the hydrolysis reaction of ampicillin and imipenem. For CENTA hydrolysis, some improvement (14ndm) or deterioration (15ndm) of the kinetic parameters was observed. A possible explanation of this phenomenon is that the Ω loop is located in close proximity of the active site of the enzyme (Fig. 8). The distance between the metal center, formed *inter alia* by Glu152, and the Zn1 and Zn2 sites is about 8 and 12 Å, respectively. Depending on the substrate, such proximity of the metal center and its macromolecular environment, including the Glu152 residue, could shield some part of the active site. Indeed, for the kinetic study of NDM-1 with the CENTA substrate containing two bulky substituents at the 3'- and 7-positions, the K_M value is three times higher as compared to the reactions with ampicillin and imipenem. Binding of CENTA is more efficient in the 14ndm variant with deleted Ω loop. On the other hand, for the second Ω loop deletion mutant with the additional M154V substitution (15ndm), ligand binding is significantly affected. Therefore, elucidation of the exact role of the Ω loop in NDM-catalyzed hydrolysis of β-lactams requires further studies.

The K_M values obtained in this work by UV-Vis absorption measurements are consistently higher than reported previously, while the k_{cat} values are lower, for both ampicillin and imipenem [39,40]. This leads to decreased catalytic efficiencies (k_{cat}/K_M) that are on average almost an order of magnitude lower than reported before. It is possible that the enzymes are

less efficient in the presence of high concentrations of Zn^{2+} ions that were used in this study [14,39,40,44]. Another possibility is that the quality of protein samples used for the kinetic experiments was suboptimal. However, sample preparation as well as the reaction conditions were identical for all the variants, which should make the results presented in this work consistent and directly comparable.

Noticeable increases in K_M values for the L3 loop mutants suggest a role of the loop in substrate binding. For ampicillin and imipenem, the largest K_M values were determined for variants with either a deletion of the entire loop (10ndm) or point mutations resulting in a double positive charge but retaining the same loop length (13ndm). However, for other variants we observed clear differences in their behavior towards these two substrates.

The high K_M value for 8ndm (ΔL65A72) with ampicillin (1914 ± 262 mM), similar to that for variant 10ndm with whole-loop deletion, suggests a specific role of Leu65, or Leu65 and Ala72 residues, in binding of ampicillin. In our crystal structure of NDM-12, as well as in the structure 5ZGE of NDM-1 containing hydrolyzed ampicillin, Leu65 forms van der Waals interactions with the phenyl ring of the ligand. However, Met67 forms similar interactions with the ligand and its deletion in 6ndm did not have such a dramatic effect on K_M. Interestingly, variant 9ndm with a four-residue deletion in loop L3 (ΔD66M67F70G71), has a similar K_M value to that of the wild-type enzymes in the reaction with ampicillin. For imipenem, both variants 8ndm and 9ndm have a very similar K_M value, which is smaller than for variant 10ndm with the whole-loop deletion but larger than for the wild-type enzyme. Another noticeable difference between these two substrates is found for variant 5ndm (ΔP68G69), whose K_M value for imipenem shows a 3-8 fold increase compared to the natural variant, while for ampicillin it remains in the same range.

Interestingly, for the majority of the mutants tested, changes in K_M are coupled with changes in k_{cat} such that the resultant catalytic efficiency (i.e., k_{cat}/K_M) remains roughly

constant. Possibly, the loop increases the affinity for the substrate by forming unspecific, hydrophobic interactions upon its binding. If these interactions persisted after the hydrolysis reaction, they would slow down product release and thus the whole enzymatic reaction. Flexibility of the L3 loop is necessary to ensure that it will be able to adopt its structure for interactions with different classes of antibiotic substrates. In our experiments, the catalytic efficiencies of loop L3 mutants are overall very similar to those of wild-type enzymes. However, at lower substrate concentrations and undersaturation of the enzyme, the variants with higher substrate affinities will perform better and process the substrate more quickly.

Sao Paulo metallo-β-lactamase, as well as class B2 enzymes, instead of a long and flexible L3 loop have an extended α3 region, which may play a similar role. This region in B2 enzymes was described as forming a 'hydrophobic wall' that contributes to substrate binding [45]. On the other hand, it was also shown that the α3 region facilitates β-lactam hydrolysis by undergoing conformational changes. Such flexible regions may provide a mechanism of adaptation of these enzymes to conditions of relatively low concentrations of the antibiotic substrate, all of which needs to be efficiently removed in order to avoid its negative effects for the bacterial cell.

The inhibition effect observed for CENTA could be caused by either the substrate itself or by the accumulated reaction product. A somewhat similar phenomenon of substrate inhibition was previously observed for B1- and B3-type MBLs, including CcrA from *Bacillus subtilis* (a member of B1 subgroup) [46] and several β-lactamases from the B3 subgroup, like MIM-1 and MIM-2 MBLs from non-pathogenic marine organisms [47] and AIM-1 imipenemase [48]. It is of note that various classes of β-lactams, including penicillines, penems and cephalosporins, affect the activity of various B1 and B3 MBLs at higher concentrations. Depending on the antibiotic/enzyme combinations, the established K_i values were in the approximate range 70 – 900 μM. The same inhibitory effect observed in two subgroups of

MBLs may be linked to similar organization of their active site (presence of loop L3 and coordination of two Zn^{2+} ions). On the other hand, the β-lactamase activity of the NDM variants analyzed in this study was affected only at higher concentrations of the CENTA cephalosporin. The estimated K_i values for CENTA are in a wide range from 170 to ~3000 μM. These values are higher than those estimated for other cephalosporins (K_i values of ~70 μM) affecting the activity of B3-type MBLs [47]. However, as mentioned before, the enzymatic activity of the NDM variants assayed within this study was suboptimal; therefore, these results should not be used for direct comparisons with other enzymes. Another possible explanation of the drop of catalytic activity of NDM variants in the presence of the chromogenic cephalosporin would be the effect of a product of CENTA hydrolysis. It has been previously reported that for cephalosporins with good leaving group at position C3', tautomerization of the dihydrothiazine ring occurs upon β-lactam hydrolysis, resulting in the formation of a new C4=N5 double bond and a shift of the existing double bond from C3=C4 to C3=C3' with the elimination of the group bound at C3' [22,49,50,51]. As shown in Fig. 7B, for the CENTA substrate the resulting 2-nitro-5-thiobenzoate product (TNB^{2-}) would have a free thiol group by which it could directly bind to the zinc center, possibly with higher affinity than the substrate. The strongest inhibition observed for 13ndm seems to support this explanation as the positively charged Lys residues could interact with the carboxylate group of the postulated product-inhibitor. However, in our crystallization experiments with TNB^{2-}, the product of DNTB reduction, we were not able to confirm binding of this fragment to NDM-1. This might be blamed on the low solubility of DTNB and thus low concentration of the inhibitor in the complex-formation reaction. Also, the Zn^{2+} ions present in the buffer could directly interact with the free thiol group of TNB^{2-} and negatively affect its binding to the enzyme.

Further experiments are needed to explain the mechanism of inhibition of NDM upon its reaction with CENTA, but there is no doubt that our observation could lead to interesting development of substrate-related inhibitors of metallo-β-lactamases.

5. Conclusions

Even extensive deletions in the L3 loop did not completely abolish the enzymatic activity of the NDM proteins tested. L3 loop mutants had increased K_M values which would impair their functioning in the conditions of low substrate concentration. Different elements of the loop play distinctive roles in the hydrolysis of different substrates. Overall, flexibility of the L3 loop seems necessary to fulfill the requirements imposed by various types of substrates. Deletions in the Ω loop significantly improved the enzymatic activity, especially for such substrates as ampicillin and imipenem. On the other hand, opposite effects on hydrolytic activity were observed for the CENTA substrate (increase or decrease of the activity for 14ndm or 5ndm variant, respectively). Further studies are needed to elucidate the role of the Ω loop in the hydrolysis of β-lactam substrates.

A dimer interface preserved in many structures with different crystal packing is supported by metal ion coordination between the two protein molecules. This could be a way to accumulate additional Zn^{2+} ions which could provide a "backup" storage when the host immune response takes effect and leads to a depletion of zinc levels.

The NDM enzymes were inhibited in the reaction with CENTA, by either the substrate itself or a product of the hydrolysis reaction. Further research is needed to explain the mechanism of this inhibition but hopefully this observation will provide a valuable hint to guide the much needed MBL inhibitor design efforts.

Conflict of interest

none declared

Author contributions

J.E.R. designed and performed biochemical experiments and structural studies, analyzed the data, and wrote the manuscript. B.I., M.K., J.S. and J.C-H. performed biochemical experiments. K.B. performed structural studies, analyzed the data and wrote the manuscript. M.J. analyzed the data and wrote the manuscript.

Acknowledgments

Work carried out within the DesInMBL project with support from the Polish National Center for Research and Development within the JPIAMR program (NCBR AMR/1/2015). X-Ray diffraction measurements were carried out at the BL14.1 beamline of the Helmholtz-Zentrum Berlin (HZB) and Petra III beamline P13, EMBL c/o DESY Hamburg. The authors thank HZB and EMBL for the allocation of synchrotron radiation beamtime and the staff for assistance at the beamlines. The authors wish to thank Dr. Jakub Barciszewski for help with X-ray diffraction data measurements and handling of raw diffraction images.

References

[1] D. Yong, M.A. Toleman, C.G. Giske, H.S. Cho, K. Sundman, K. Lee, T.R. Walsh, Characterization of a New Metallo-β-Lactamase Gene, blaNDM-1, and a Novel Erythromycin Esterase Gene Carried on a Unique Genetic Structure in *Klebsiella pneumoniae* Sequence Type 14 from India, Antimicrob. Agents Chemother. 53 (2009) 5046–5054. https://doi.org/10.1128/AAC.00774-09.

[2] T. Palzkill, Metallo-β-lactamase structure and function: Metallo-β-lactamase structure and function, Ann. N. Y. Acad. Sci. 1277 (2013) 91–104. https://doi.org/10.1111/j.1749-6632.2012.06796.x.

[3] J. Wachino, Y. Yamaguchi, S. Mori, H. Kurosaki, Y. Arakawa, K. Shibayama, Structural insights into the subclass B3 metallo-β-lactamase SMB-1 and the mode of inhibition by the common metallo-β-lactamase inhibitor mercaptoacetate, Antimicrob. Agents Chemother. 57 (2013) 101–109. https://doi.org/10.1128/AAC.01264-12.

[4] J. Brem, W.B. Struwe, A.M. Rydzik, H. Tarhonskaya, I. Pfeffer, E. Flashman, S.S. van Berkel, J. Spencer, T.D.W. Claridge, M.A. McDonough, J.L.P. Benesch, C.J. Schofield,

Studying the active-site loop movement of the São Paolo metallo-β-lactamase-1, Chem. Sci. 6 (2015) 956–963. https://doi.org/10.1039/C4SC01752H.
[5] M.W. Crowder, J. Spencer, A.J. Vila, Metallo-β-lactamases: novel weaponry for antibiotic resistance in bacteria, Acc. Chem. Res. 39 (2006) 721–728. https://doi.org/10.1021/ar0400241.
[6] C. Bebrone, Metallo-β-lactamases (classification, activity, genetic organization, structure, zinc coordination) and their superfamily, Biochem. Pharmacol. 74 (2007) 1686–1701. https://doi.org/10.1016/j.bcp.2007.05.021.
[7] M.I. Page, A. Badarau, The Mechanisms of Catalysis by Metallo-β-Lactamases, Bioinorg. Chem. Appl. 2008 (2008) 1–14. https://doi.org/10.1155/2008/576297.
[8] H.-K.S. Leiros, P.S. Borra, B.O. Brandsdal, K.S.W. Edvardsen, J. Spencer, T.R. Walsh, O. Samuelsen, Crystal structure of the mobile metallo-β-lactamase AIM-1 from *Pseudomonas aeruginosa*: insights into antibiotic binding and the role of Gln157, Antimicrob. Agents Chemother. 56 (2012) 4341–4353. https://doi.org/10.1128/AAC.00448-12.
[9] N. Mitić, M. Miraula, C. Selleck, K.S. Hadler, E. Uribe, M.M. Pedroso, G. Schenk, Catalytic mechanisms of metallohydrolases containing two metal ions, Adv. Protein Chem. Struct. Biol. 97 (2014) 49–81. https://doi.org/10.1016/bs.apcsb.2014.07.002.
[10] E.K. Phelan, M. Miraula, C. Selleck, D.L. Ollis, G. Schenk, N. Mitić, Metallo-β-Lactamases: A Major Threat to Human Health, Am. J. Mol. Biol. 04 (2014) 89–104. https://doi.org/10.4236/ajmb.2014.43011.
[11] P. Hinchliffe, M.M. González, M.F. Mojica, J.M. González, V. Castillo, C. Saiz, M. Kosmopoulou, C.L. Tooke, L.I. Llarrull, G. Mahler, R.A. Bonomo, A.J. Vila, J. Spencer, Cross-class metallo-β-lactamase inhibition by bisthiazolidines reveals multiple binding modes, Proc. Natl. Acad. Sci. U. S. A. 113 (2016) E3745-3754. https://doi.org/10.1073/pnas.1601368113.
[12] Y. Kim, C. Tesar, J. Mire, R. Jedrzejczak, A. Binkowski, G. Babnigg, J. Sacchettini, A. Joachimiak, Structure of Apo- and Monometalated Forms of NDM-1—A Highly Potent Carbapenem-Hydrolyzing Metallo-β-Lactamase, PLoS ONE. 6 (2011) e24621. https://doi.org/10.1371/journal.pone.0024621.
[13] D. King, N. Strynadka, Crystal structure of New Delhi metallo-β-lactamase reveals molecular basis for antibiotic resistance, Protein Sci. 20 (2011) 1484–1491. https://doi.org/10.1002/pro.697.
[14] A.R. Palacios, M.F. Mojica, E. Giannini, M.A. Taracila, C.R. Bethel, P.M. Alzari, L.H. Otero, S. Klinke, L.I. Llarrull, R.A. Bonomo, A.J. Vila, The Reaction Mechanism of Metallo-β-Lactamases Is Tuned by the Conformation of an Active-Site Mobile Loop, Antimicrob. Agents Chemother. 63 (2019) e01754-18. https://doi.org/10.1128/AAC.01754-18.
[15] J.M. González, A. Buschiazzo, A.J. Vila, Evidence of Adaptability in Metal Coordination Geometry and Active-Site Loop Conformation among B1 Metallo-β-lactamases, Biochemistry. 49 (2010) 7930–7938. https://doi.org/10.1021/bi100894r.
[16] C. Moali, C. Anne, J. Lamotte-Brasseur, S. Groslambert, B. Devreese, J. Van Beeumen, M. Galleni, J.-M. Frère, Analysis of the Importance of the Metallo-β-Lactamase Active Site Loop in Substrate Binding and Catalysis, Chem. Biol. 10 (2003) 319–329. https://doi.org/10.1016/S1074-5521(03)00070-X.
[17] S.D.B. Scrofani, J. Chung, J.J.A. Huntley, S.J. Benkovic, P.E. Wright, H.J. Dyson, NMR Characterization of the Metallo-β-lactamase from *Bacteroides fragilis* and Its Interaction with a Tight-Binding Inhibitor: Role of an Active-Site Loop †, Biochemistry. 38 (1999) 14507–14514. https://doi.org/10.1021/bi990986t.

[18] H. Zhang, G. Ma, Y. Zhu, L. Zeng, A. Ahmad, C. Wang, B. Pang, H. Fang, L. Zhao, Q. Hao, Active-Site Conformational Fluctuations Promote the Enzymatic Activity of NDM-1, Antimicrob. Agents Chemother. 62 (2018) e01579-18. https://doi.org/10.1128/AAC.01579-18.
[19] Y. Kim, M.A. Cunningham, J. Mire, C. Tesar, J. Sacchettini, A. Joachimiak, NDM-1, the ultimate promiscuous enzyme: substrate recognition and catalytic mechanism, FASEB J. 27 (2013) 1917–1927. https://doi.org/10.1096/fj.12-224014.
[20] D.T. King, L.J. Worrall, R. Gruninger, N.C.J. Strynadka, New Delhi Metallo-β-Lactamase: Structural Insights into β-Lactam Recognition and Inhibition, J. Am. Chem. Soc. 134 (2012) 11362–11365. https://doi.org/10.1021/ja303579d.
[21] J.E. Raczynska, I.G. Shabalin, W. Minor, A. Wlodawer, M. Jaskolski, A close look onto structural models and primary ligands of metallo-β-lactamases, Drug Resist. Updat. 40 (2018) 1–12. https://doi.org/10.1016/j.drup.2018.08.001.
[22] H. Feng, J. Ding, D. Zhu, X. Liu, X. Xu, Y. Zhang, S. Zang, D.-C. Wang, W. Liu, Structural and Mechanistic Insights into NDM-1 Catalyzed Hydrolysis of Cephalosporins, J. Am. Chem. Soc. 136 (2014) 14694–14697. https://doi.org/10.1021/ja508388e.
[23] M. Aitha, A.J. Moller, I.D. Sahu, M. Horitani, D.L. Tierney, M.W. Crowder, Investigating the position of the hairpin loop in New Delhi metallo-β-lactamase, NDM-1, during catalysis and inhibitor binding, J. Inorg. Biochem. 156 (2016) 35–39. https://doi.org/10.1016/j.jinorgbio.2015.10.011.
[24] W. Wu, Y. Feng, G. Tang, F. Qiao, A. McNally, Z. Zong, NDM Metallo-β-Lactamases and Their Bacterial Producers in Health Care Settings, Clin. Microbiol. Rev. 32 (2019) e00115-18. https://doi.org/10.1128/CMR.00115-18.
[25] Z. Liu, A. Piccirilli, D. Liu, W. Li, Y. Wang, J. Shen, Deciphering the Role of V88L Substitution in NDM-24 metallo-β-lactamase, Catalysts. 9 (2019) 744. https://doi.org/10.3390/catal9090744.
[26] H.M. Zhang, Q. Hao, Crystal structure of NDM-1 reveals a common β-lactam hydrolysis mechanism, FASEB J. 25 (2011) 2574–2582. https://doi.org/10.1096/fj.11-184036.
[27] A.C. Stewart, C.R. Bethel, J. VanPelt, A. Bergstrom, Z. Cheng, C.G. Miller, C. Williams, R. Poth, M. Morris, O. Lahey, J.C. Nix, D.L. Tierney, R.C. Page, M.W. Crowder, R.A. Bonomo, W. Fast, Clinical Variants of New Delhi Metallo-β-Lactamase Are Evolving To Overcome Zinc Scarcity, ACS Infect. Dis. 3 (2017) 927–940. https://doi.org/10.1021/acsinfecdis.7b00128.
[28] G. Kumar, B. Issa, D. Kar, S. Biswal, A.S. Ghosh, E152A substitution drastically affects NDM-5 activity, FEMS Microbiol. Lett. (2017) fnx008. https://doi.org/10.1093/femsle/fnx008.
[29] W. Kabsch, *XDS*, Acta Crystallogr. D Biol. Crystallogr. 66 (2010) 125–132. https://doi.org/10.1107/S0907444909047337.
[30] S. French, K. Wilson, On the treatment of negative intensity observations, Acta Crystallogr. Sect. A. 34 (1978) 517–525. https://doi.org/10.1107/S0567739478001114.
[31] M.D. Winn, C.C. Ballard, K.D. Cowtan, E.J. Dodson, P. Emsley, P.R. Evans, R.M. Keegan, E.B. Krissinel, A.G.W. Leslie, A. McCoy, S.J. McNicholas, G.N. Murshudov, N.S. Pannu, E.A. Potterton, H.R. Powell, R.J. Read, A. Vagin, K.S. Wilson, Overview of the CCP4 suite and current developments, Acta Crystallogr. D Biol. Crystallogr. 67 (2011) 235–242. https://doi.org/10.1107/S0907444910045749.
[32] A.J. McCoy, R.W. Grosse-Kunstleve, P.D. Adams, M.D. Winn, L.C. Storoni, R.J. Read, *Phaser* crystallographic software, J. Appl. Crystallogr. 40 (2007) 658–674. https://doi.org/10.1107/S0021889807021206.

[33] G.N. Murshudov, P. Skubák, A.A. Lebedev, N.S. Pannu, R.A. Steiner, R.A. Nicholls, M.D. Winn, F. Long, A.A. Vagin, *REFMAC* 5 for the refinement of macromolecular crystal structures, Acta Crystallogr. D Biol. Crystallogr. 67 (2011) 355–367. https://doi.org/10.1107/S0907444911001314.
[34] P. Emsley, B. Lohkamp, W.G. Scott, K. Cowtan, Features and development of *Coot*, Acta Crystallogr. D Biol. Crystallogr. 66 (2010) 486–501. https://doi.org/10.1107/S0907444910007493.
[35] W.L. DeLano, The PyMOL Molecular Graphics System, Version 1.8, Schrödinger, LLC.
[36] V.B. Chen, W.B. Arendall, J.J. Headd, D.A. Keedy, R.M. Immormino, G.J. Kapral, L.W. Murray, J.S. Richardson, D.C. Richardson, *MolProbity* : all-atom structure validation for macromolecular crystallography, Acta Crystallogr. D Biol. Crystallogr. 66 (2010) 12–21. https://doi.org/10.1107/S0907444909042073.
[37] H. Berman, K. Henrick, H. Nakamura, Announcing the worldwide Protein Data Bank, Nat. Struct. Biol. 10 (2003) 980–980. https://doi.org/10.1038/nsb1203-980.
[38] H.M. Berman, The Protein Data Bank, Nucleic Acids Res. 28 (2000) 235–242. https://doi.org/10.1093/nar/28.1.235.
[39] A. Makena, J. Brem, I. Pfeffer, R.E.J. Geffen, S.E. Wilkins, H. Tarhonskaya, E. Flashman, L.M. Phee, D.W. Wareham, C.J. Schofield, Biochemical characterization of New Delhi metallo-β-lactamase variants reveals differences in protein stability, J. Antimicrob. Chemother. 70 (2015) 463–469. https://doi.org/10.1093/jac/dku403.
[40] Z. Cheng, P.W. Thomas, L. Ju, A. Bergstrom, K. Mason, D. Clayton, C. Miller, C.R. Bethel, J. VanPelt, D.L. Tierney, R.C. Page, R.A. Bonomo, W. Fast, M.W. Crowder, Evolution of New Delhi metallo-β-lactamase (NDM) in the clinic: Effects of NDM mutations on stability, zinc affinity, and mono-zinc activity, J. Biol. Chem. 293 (2018) 12606–12618. https://doi.org/10.1074/jbc.RA118.003835.
[41] P. Müller, S. Köpke, G.M. Sheldrick, Is the bond-valence method able to identify metal atoms in protein structures?, Acta Crystallogr. D Biol. Crystallogr. 59 (2003) 32–37. https://doi.org/10.1107/S0907444902018000.
[42] H. Zheng, D.R. Cooper, P.J. Porebski, I.G. Shabalin, K.B. Handing, W. Minor, *CheckMyMetal* : a macromolecular metal-binding validation tool, Acta Crystallogr. Sect. Struct. Biol. 73 (2017) 223–233. https://doi.org/10.1107/S2059798317001061.
[43] H. Feng, X. Liu, S. Wang, J. Fleming, D.-C. Wang, W. Liu, The mechanism of NDM-1-catalyzed carbapenem hydrolysis is distinct from that of penicillin or cephalosporin hydrolysis, Nat. Commun. 8 (2017) 2242. https://doi.org/10.1038/s41467-017-02339-w.
[44] P.W. Thomas, M. Zheng, S. Wu, H. Guo, D. Liu, D. Xu, W. Fast, Characterization of Purified New Delhi Metallo-β-lactamase-1, Biochemistry. 50 (2011) 10102–10113. https://doi.org/10.1021/bi201449r.
[45] G. Garau, C. Bebrone, C. Anne, M. Galleni, J.-M. Frère, O. Dideberg, A Metallo-β-lactamase Enzyme in Action: Crystal Structures of the Monozinc Carbapenemase CphA and its Complex with Biapenem, J. Mol. Biol. 345 (2005) 785–795. https://doi.org/10.1016/j.jmb.2004.10.070.
[46] M.P. Yanchak, R.A. Taylor, M.W. Crowder, Mutational analysis of metallo-β-lactamase CcrA from *Bacteroides fragilis*, Biochemistry. 39 (2000) 11330–11339. https://doi.org/10.1021/bi0010524.
[47] M. Miraula, J.J. Whitaker, G. Schenk, N. Mitić, β-Lactam antibiotic-degrading enzymes from non-pathogenic marine organisms: a potential threat to human health, J. Biol. Inorg. Chem. 20 (2015) 639–651. https://doi.org/10.1007/s00775-015-1250-x.

[48] C. Selleck, J.A. Larrabee, J. Harmer, L.W. Guddat, N. Mitić, W. Helweh, D.L. Ollis, W.R. Craig, D.L. Tierney, M. Monteiro Pedroso, G. Schenk, AIM-1: An Antibiotic-Degrading Metallohydrolase That Displays Mechanistic Flexibility, Chem. Eur. J. 22 (2016) 17704–17714. https://doi.org/10.1002/chem.201602762.
[49] W.S. Faraci, R.F. Pratt, Elimination of a good leaving group from the 3'-position of a cephalosporin need not be concerted with .beta.-lactam ring opening: TEM-2 .beta.-lactamase-catalyzed hydrolysis of pyridine-2-azo-4'-(N',N'-dimethylaniline) cephalosporin (PADAC) and of cephaloridine, J. Am. Chem. Soc. 106 (1984) 1489–1490. https://doi.org/10.1021/ja00317a053.
[50] R.F. Pratt, W.S. Faraci, Direct observation by proton NMR of cephalosporoate intermediates in aqueous solution during the hydrazinolysis and .beta.-lactamase-catalyzed hydrolysis of cephalosporins with 3' leaving groups: kinetics and equilibria of the 3' elimination reaction, J. Am. Chem. Soc. 108 (1986) 5328–5333. https://doi.org/10.1021/ja00277a044.
[51] J.L. Olmos, S. Pandey, J.M. Martin-Garcia, G. Calvey, A. Katz, J. Knoska, C. Kupitz, M.S. Hunter, M. Liang, D. Oberthuer, O. Yefanov, M. Wiedorn, M. Heyman, M. Holl, K. Pande, A. Barty, M.D. Miller, S. Stern, S. Roy-Chowdhury, J. Coe, N. Nagaratnam, J. Zook, J. Verburgt, T. Norwood, I. Poudyal, D. Xu, J. Koglin, M.H. Seaberg, Y. Zhao, S. Bajt, T. Grant, V. Mariani, G. Nelson, G. Subramanian, E. Bae, R. Fromme, R. Fung, P. Schwander, M. Frank, T.A. White, U. Weierstall, N. Zatsepin, J. Spence, P. Fromme, H.N. Chapman, L. Pollack, L. Tremblay, A. Ourmazd, G.N. Phillips, M. Schmidt, Enzyme intermediates captured "on the fly" by mix-and-inject serial crystallography, BMC Biol. 16 (2018) 59. https://doi.org/10.1186/s12915-018-0524-5.
[52] R.A. Laskowski, J. Jabłońska, L. Pravda, R.S. Vařeková, J.M. Thornton, PDBsum: Structural summaries of PDB entries, Protein Sci. 27 (2018) 129–134. https://doi.org/10.1002/pro.3289.
[53] C.S. Bond, TopDraw: a sketchpad for protein structure topology cartoons, Bioinformatics. 19 (2003) 311–312. https://doi.org/10.1093/bioinformatics/19.2.311.

Table 1. Kinetic parameters of ampicillin hydrolysis.

Enzyme variant	**K_M [μM]**	**k_{cat} [s^{-1}]**	**k_{cat}/K_M [$\mu M^{-1} \cdot s^{-1}$]**
NDM-1	395 ± 109	592 ± 38	1.50 ± 0.42
NDM-9	578 ± 102	221 ± 12	0.38 ± 0.07
NDM-11	958 ± 174	591 ± 44	0.62 ± 0.12
NDM-12	935 ± 113	387 ± 18	0.41 ± 0.05
14ndm-ΔQ151E152M154	62 ± 18	28 ± 1	0.45 ± 0.13
15ndm-M154V-ΔQ151E152	19 ± 11	27 ± 1	1.42 ± 0.82
5ndm-ΔP68G69	770 ± 84	350 ± 114	0.45 ± 0.16
6ndm-ΔM67F70	1114 ± 100	354 ± 14	0.32 ± 0.03
7ndm-ΔD66G71	1129 ± 148	453 ± 26	0.40 ± 0.06
8ndm-ΔL65A72	1914 ± 262	564 ± 41	0.29 ± 0.05
9ndm-ΔD66M67F70G71	515 ± 64	232 ± 8	0.45 ± 0.06
10ndm-ΔL65D66M67F70G71A72	2167 ± 342	380 ± 33	0.18 ± 0.03
11ndm-M67N-F70N	755 ± 68	380 ± 14	0.50 ± 0.05
12ndm-D66N-M67E-F70E	734 ± 107	329 ± 17	0.45 ± 0.07
13ndm-D66N-M67K-F70K	2456 ± 364	832 ± 71	0.34 ± 0.06

Table 2. Kinetic parameters of imipenem hydrolysis.

Enzyme variant	**K_M [μM]**	**k_{cat} [s^{-1}]**	**k_{cat}/K_M [$\mu M^{-1} \cdot s^{-1}$]**
NDM-1	296 ± 20	136 ± 3	0.46 ± 0.03
NDM-9	410 ± 49	126 ± 6	0.31 ± 0.04
NDM-11	162 ± 31	77 ± 3	0.48 ± 0.09
NDM-12	151 ± 21	74 ± 2	0.49 ± 0.07
14ndm-ΔQ151E152M154	209 ± 30	36 ± 1	0.17 ± 0.03
15ndm-M154V-ΔQ151E152	63 ± 11	23 ± 1	0.36 ± 0.07
5ndm-ΔP68G69	1203 ± 138	329 ± 22	0.27 ± 0.04
6ndm-ΔM67F70	873 ± 191	210 ± 22	0.24 ± 0.06
7ndm-ΔD66G71	866 ± 126	190 ± 14	0.22 ± 0.04
8ndm-ΔL65A72	1501 ± 190	411 ± 32	0.27 ± 0.04
9ndm-ΔD66M67F70G71	1376 ± 211	270 ± 24	0.20 ± 0.03
10ndm-ΔL65D66M67F70G71A72	1929 ± 579	396 ± 79	0.21 ± 0.07
11ndm-M67N-F70N	701 ± 140	227 ± 19	0.32 ± 0.07
12ndm-D66N-M67E-F70E	1192 ± 301	225 ± 31	0.19 ± 0.05
13ndm-D66N-M67K-F70K	2812 ± 469	355 ± 41	0.13 ± 0.03

Table 3. Kinetic parameters of CENTA hydrolysis. K_i values correspond to inhibition by substrate.

Enzyme variant	**K_M [μM]**	**k_{cat} [s^{-1}]**	**k_{cat}/K_M [$\mu M^{-1} \cdot s^{-1}$]**	**K_i [μM]**
NDM-1	937 ± 173	58 ± 8	0.06 ± 0.01	459 ± 92
NDM-9	1021 ± 114	85 ± 7	0.08 ± 0.01	476 ± 54
NDM-11	906 ± 180	70 ± 1	0.08 ± 0.02	549 ± 121
NDM-12	1002 ± 158	56 ± 6	0.06 ± 0.01	660 ± 114
14ndm-ΔQ151E152M154	686 ± 189	22 ± 4	0.03 ± 0.01	899 ± 493
15ndm-M154V-ΔQ151E152	1782 ± 784	48 ± 2	0.03 ± 0.01	301 ± 135
5ndm-ΔP68G69	1032 ± 139	43 ± 4	0.04 ± 0.01	1104 ± 198
6ndm-ΔM67F70	2420 ± 503	101 ± 18	0.04 ± 0.01	533 ± 138
7ndm-ΔD66G71	1016 ± 269	32 ± 6	0.03 ± 0.01	1316 ± 864
8ndm-ΔL65A72	432 ± 158	30 ± 6	0.07 ± 0.03	1994 ± 860
9ndm-ΔD66M67F70G71	281 ± 67	39 ± 4	0.14 ± 0.04	3057 ± 1015
10ndm-ΔL65D66M67F70G71A72	406 ± 42	11 ± 1	0.03 ± 0.01	-
11ndm-M67N-F70N	1304 ± 858	66 ± 34	0.05 ± 0.04	496 ± 318
12ndm-D66N-M67E-F70E	1171 ± 910	67 ± 41	0.06 ± 0.06	607 ± 569
13ndm-D66N-M67K-F70K	2082 ± 745	83 ± 25	0.04 ± 0.02	170 ± 69

Table 4. X-Ray data collection and refinement statistics.

	NDM-12/amp	**NDM-9**	**NDM-1**
Data collection			
Space group	$P2_12_12_1$	$P3_1$	$P2_12_12_1$
Cell parameters [Å]	a=38.5 b=76.4 c=130.9	a=b=122.9 c=38.5	a=70.5 b=74.0 c=77.7
Temperature [K]	100	100	100
Resolution [Å]	2.10 (2.23-2.10)[1]	1.43 (1.52-1.43)	0.95 (1.00-0.95)
Completeness [%]	97.6 (96.6)	99.8 (98.8)	99.8 (98.8)
$CC_{1/2}$	0.99 (0.62)	0.99 (0.71)	0.99 (0.63)
$\langle I/\sigma \rangle$	7.0 (1.4)	16.5 (2.6)	20.4 (1.4)
Unique reflections	22766	120213	253370
Data redundancy	4.3 (3.9)	10.4 (10.4)	12.9 (12.1)
R_{meas}	0.169 (0.917)	0.088 (0.782)	0.064 (1.631)
Refinement			
No. of reflections, refinement/R_{free}	21606/1160	117209/3004	252356/1014
R/R_{free}	0.172/0.227	0.074/0.116	0.105/0.120
Protein molecules in ASU	2	3	2
ADP parametrization	Isotropic + TLS	anisotropic	anisotropic
No. atoms, protein/water/other	3605/231/61	5169/778/99	3624/574/27
Ramachandran angles, favored/allowed/outliers [%]	97.9/2.1/0.0	99.0/1.0/0.0	99.0/1.0/0.0
Average B factor [Å^2]	36.4	22.5	14.0
PDB accession code	6OL8	6OGO	6TWT

[1]Values in parentheses are for highest resolution shell.

Figure 1. Topology diagram of NDM-1 based on the 5ZGE model [26]. The β-strands (yellow arrows) and helices (red cylinders) are numbered consecutively. The inclusive residue numbers correspond to secondary structure assignments in *PDBsum* database [52]. Two accessory loop regions discussed in this paper, namely L3 and Ω, that are present in numerous variants of NDM are highlighted in blue and green, respectively. This topology diagram was prepared in *TopDraw* [53].

Figure 2. (A) Sequence alignment of several B1 metallo-β-lactamases showing the L3 loop (shaded area) and neighboring residues. The sequences of the following MBLs were acquired from GenBank (Benson *et al.*, 2013; sequence identifiers in parentheses): NDM-1 (CAZ39946.1), VIM-1 (CAB46686.1), IMP-1 (AAB30289.1), BcII-1 (AAA22276.1), CfiA (AAA22907.1), SFB-1 (AAT90847.1), SLB-1 (AAT90846.1), KHM-1 (BAH16555.1), SIM-1 (AAX76774.1), GIM-1 (CAF05908.1), DIM-1 (ADD91577.1), TMB-1 (CBY88906.1), FIM-1 (AFV91534.1), MUS-1 (AAN63647.1), TUS-1 (AAN63648.1), EBR-1 (AAN32638.1), IND-1 (AAD20273.1), BlaB-1 (AAF89154.1), JOHN-1 (AAK38324.1) and SPM-1 (AAR15341.1). (B) Structure-based sequence alignment of NDM-1 and SPM-1 within the α4-β9 region. The shaded area indicates the actual Ω loop in NDM-1. (C) and (D) Sequences of NDM variants presented in this study with mutations within L3 (C) and α4-β8 (D) loops. The L3 and Ω loop variable regions are shaded. Underlined numbers denote acronyms of the studied mutants as defined in the Introduction. Numbering corresponds to the sequence of NDM-1.

Figure 3. Structural alignment of five (A) or four (B) independent protein subunits from the crystal structures of NDM 1: PDB ID 3SPU (A) or its mutant PDB ID 6ACA (B), showing

different conformations of the L3 loop (top right corner). (C) Interactions between hydrolyzed ampicillin (dark brown), bound in the NDM-1 structure 5ZGE, and loop L3 (salmon), both shown in space-filling representation. (D) and (E) Interactions between hydrolyzed ampicillin (dark brown or dark green), bound in the NDM-1 structure 5ZGE, and loop L3, both shown in space-filling representation, from the same (salmon) and a symmetry related protein molecule (green).

Figure 4. Kinetic data for CENTA hydrolysis. (A) and (B) data for the natural variants NDM-9 (A) and NDM-11 (B) showing similar inhibition effect. (C) No observable inhibition for variant 10ndm with entire L3 loop deleted. (D) Strongest inhibition effect for variant 13ndm with engineered double positive charge in loop L3.

Figure 5. (A) Alignment of the structure of NDM-12 (this work, red) with NDM-1 (PDB ID: 5ZGE, beige) crystallized with hydrolyzed ampicillin (hAmp), showing similar interactions between the bound ligand and loop L3* from a symmetry-related molecule. Asp222 residue (Gly222 in NDM-1) is shown as sticks. (B) Alignment of the present NDM-1 structure (green and yellow) with the PDB structure 5ZGE (blue and beige). Both protein chains present in the asymmetric unit align perfectly with each other (bottom of the Figure), while the symmetry-related molecules in the two structures (top right) are rotated by 57° around the b axis .

Figure 6. (A) The active site of NDM-9 with bound posphate (P_i, orange sticks) and chloride ion (green sphere). Zn^{2+} ions are shown as gray spheres. The $2mF_o$-DF_c electron density map is contoured at 1.5σ. (B) A detailed view of the interactions at the active site of NDM-9.

Arg45* from a symmetry-related molecule (light pink) forms a salt bridge with the phosphate ion. Asp124 does not interact with the zinc ions but forms a hydrogen bond with the phosphate anion, which is most likely partly protonated (HPO_4^{2-}). (C) and (D) alignement of the structures of NDM-9 (purple) and NDM-12 (orange) showing differences in the active site (C) and a similar conformation of the L3 loop except for the Phe70 side chain (D).

Figure 7. (A) Reduction of DTNB and dissociation of the resultant TNB^- product to TNB^{2-}. (B) Hydrolysis of CENTA β-lactam catalyzed by MBL. Tautomerization of the dihydrothiazine ring upon hydrolysis of the β-lactam ring would result in elimination of the fragment shown in blue (based on Feng et al. [22])

Figure 8. Calcium ion (green sphere) coordination site in the crystal structure of NDM-1 (this work, PDB ID: 6TWT) formed in part by Glu152 form the Ω loop located close to the Zn1 and Zn2 sites (gray spheres). Water molecules (Wat) are presented as red spheres. The position of hydrolased ampicillin (hAmp) was obtained by superposition of the apo (PDB ID: 6TWT) and ligand-bound (PDB ID: 5ZGE) forms of NDM-1. The coordination sphere of this intermolecular calcium binding site is completed by Glu227 from a second protein molecule (orange).

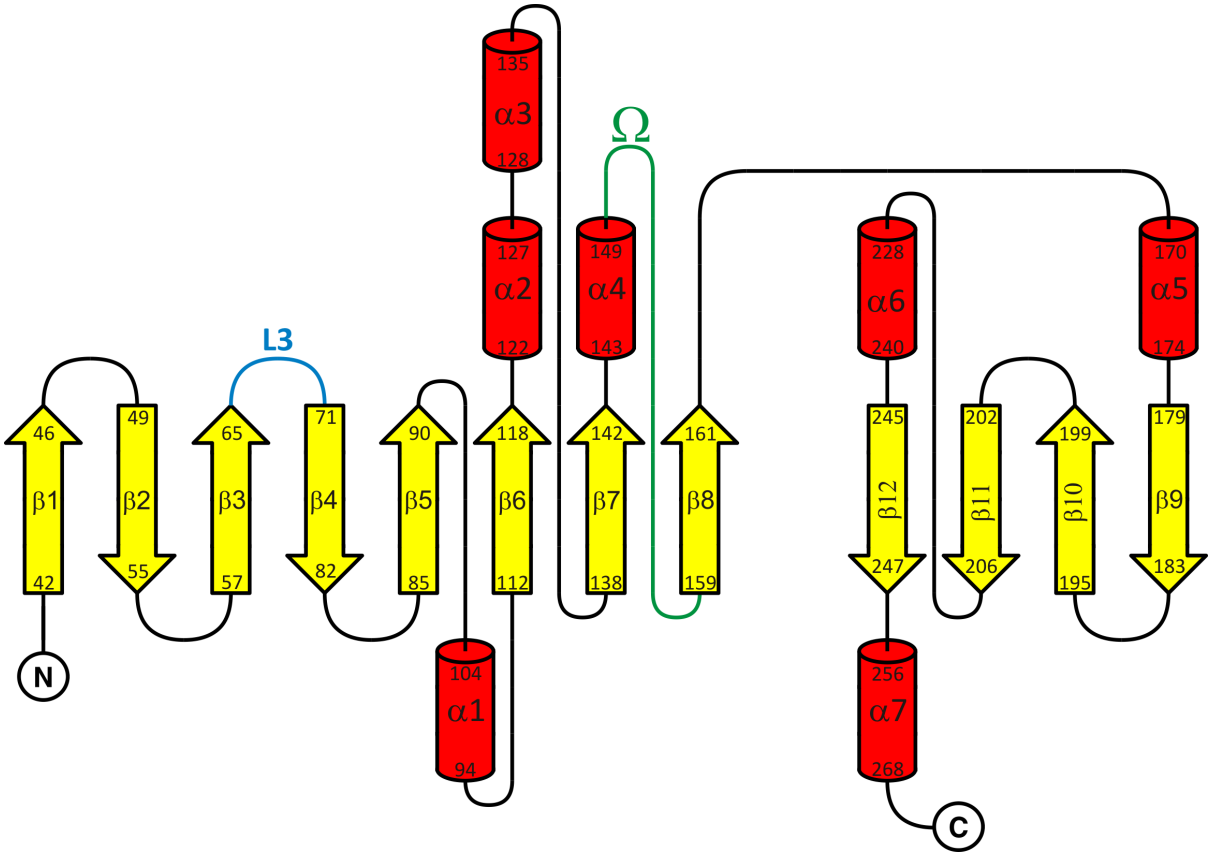

International Journal of Biological Macromolecules

Joanna Raczynska et al.

Figure 1

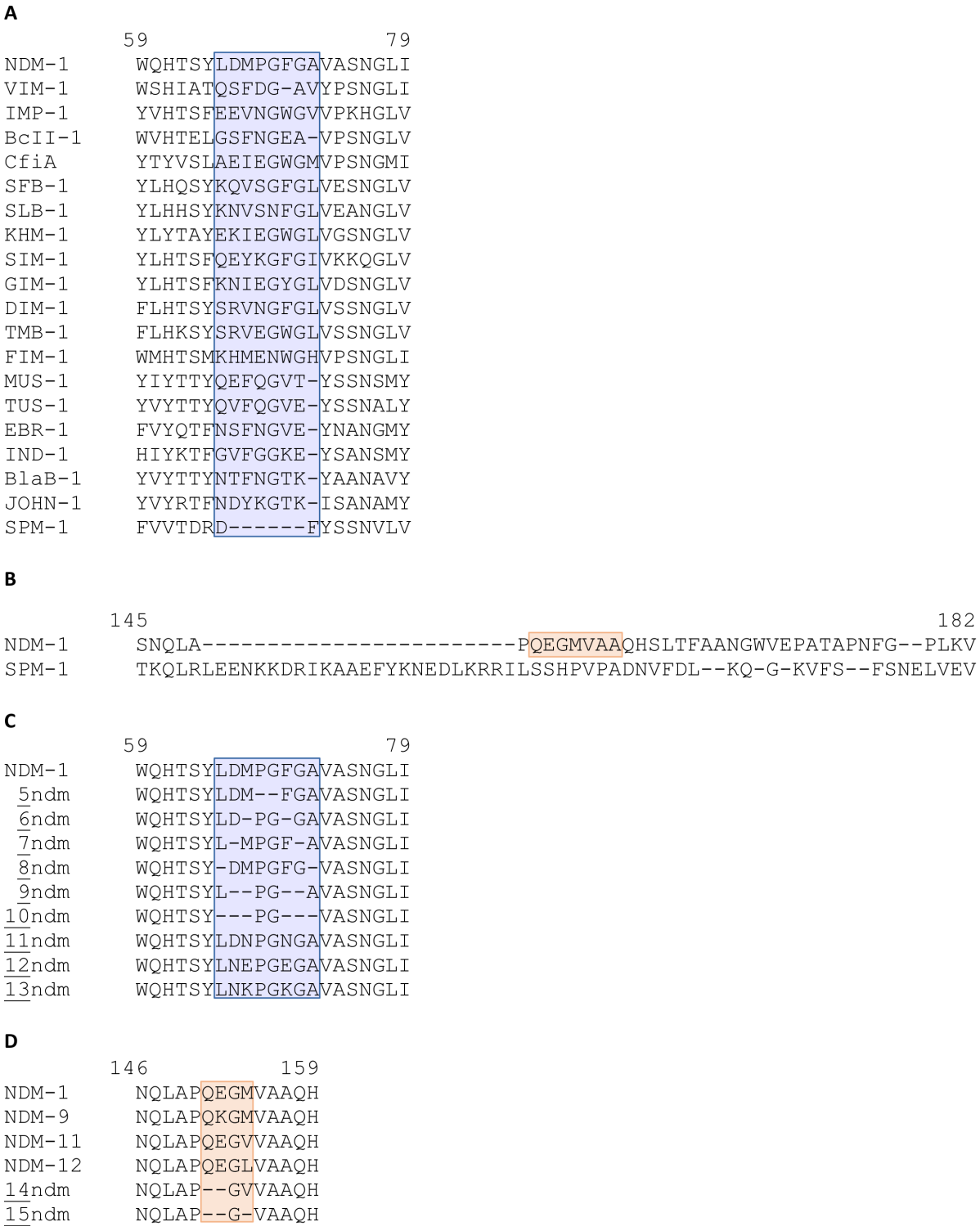

International Journal of Biological Macromolecules

Joanna Raczynska et al.

Figure 2.

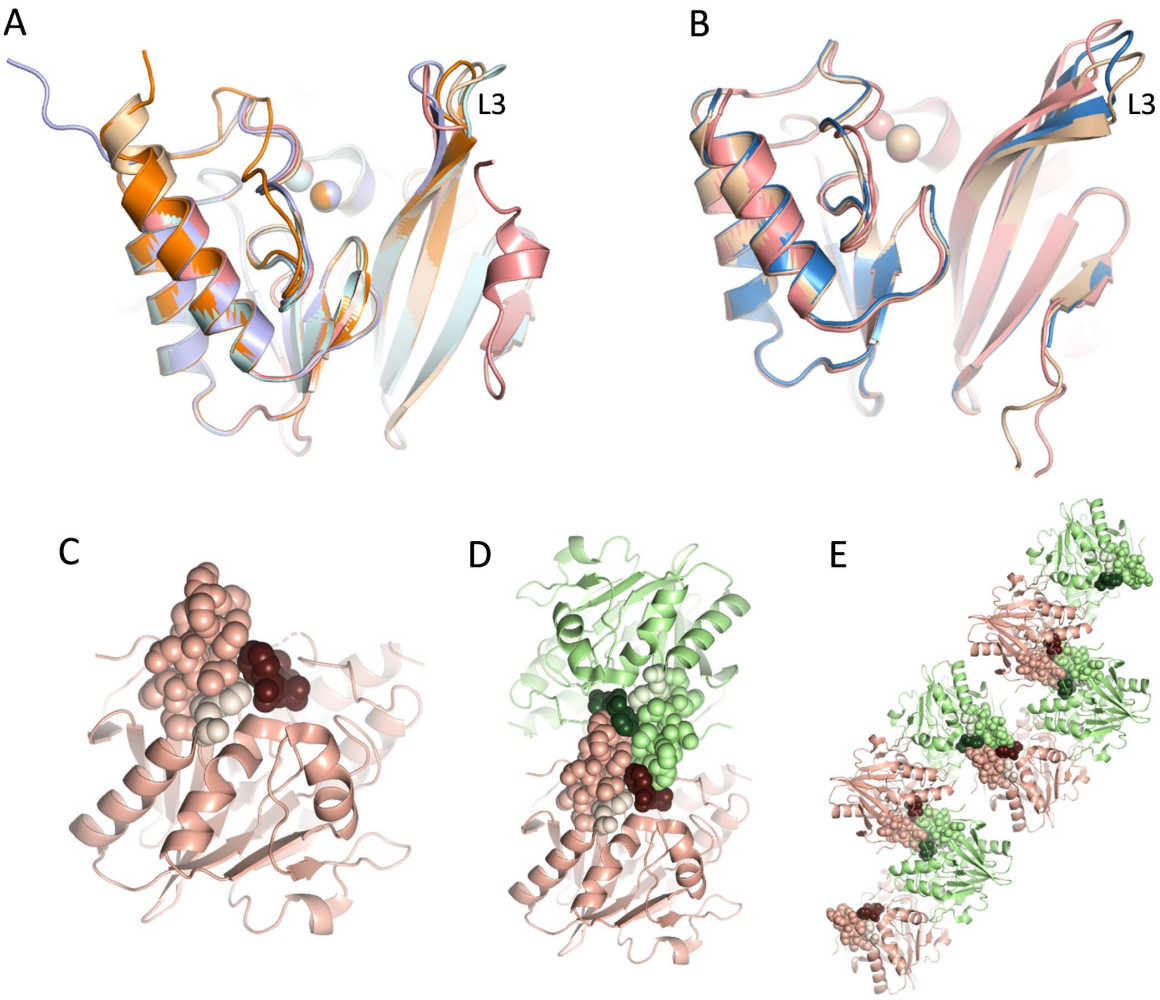

International Journal of Biological Macromolecules

Joanna Raczynska et al.

Figure 3.

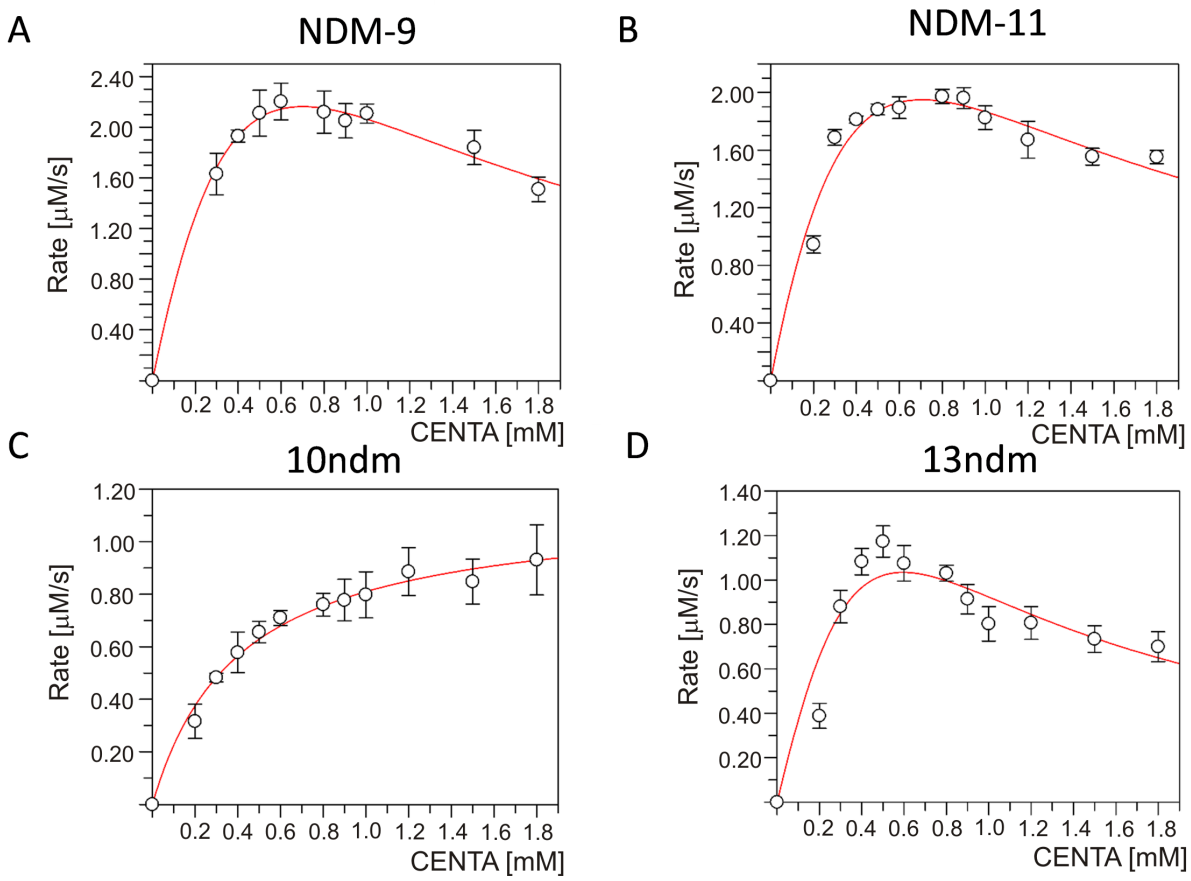

International Journal of Biological Macromolecules

Joanna Raczynska et al.

Figure 4.

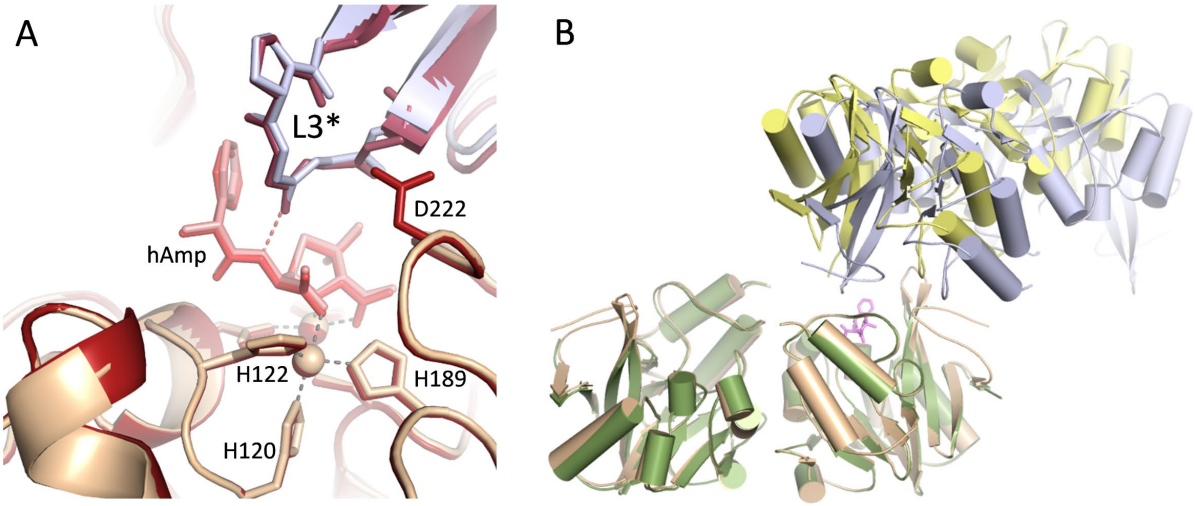

International Journal of Biological Macromolecules

Joanna Raczynska et al.

Figure 5.

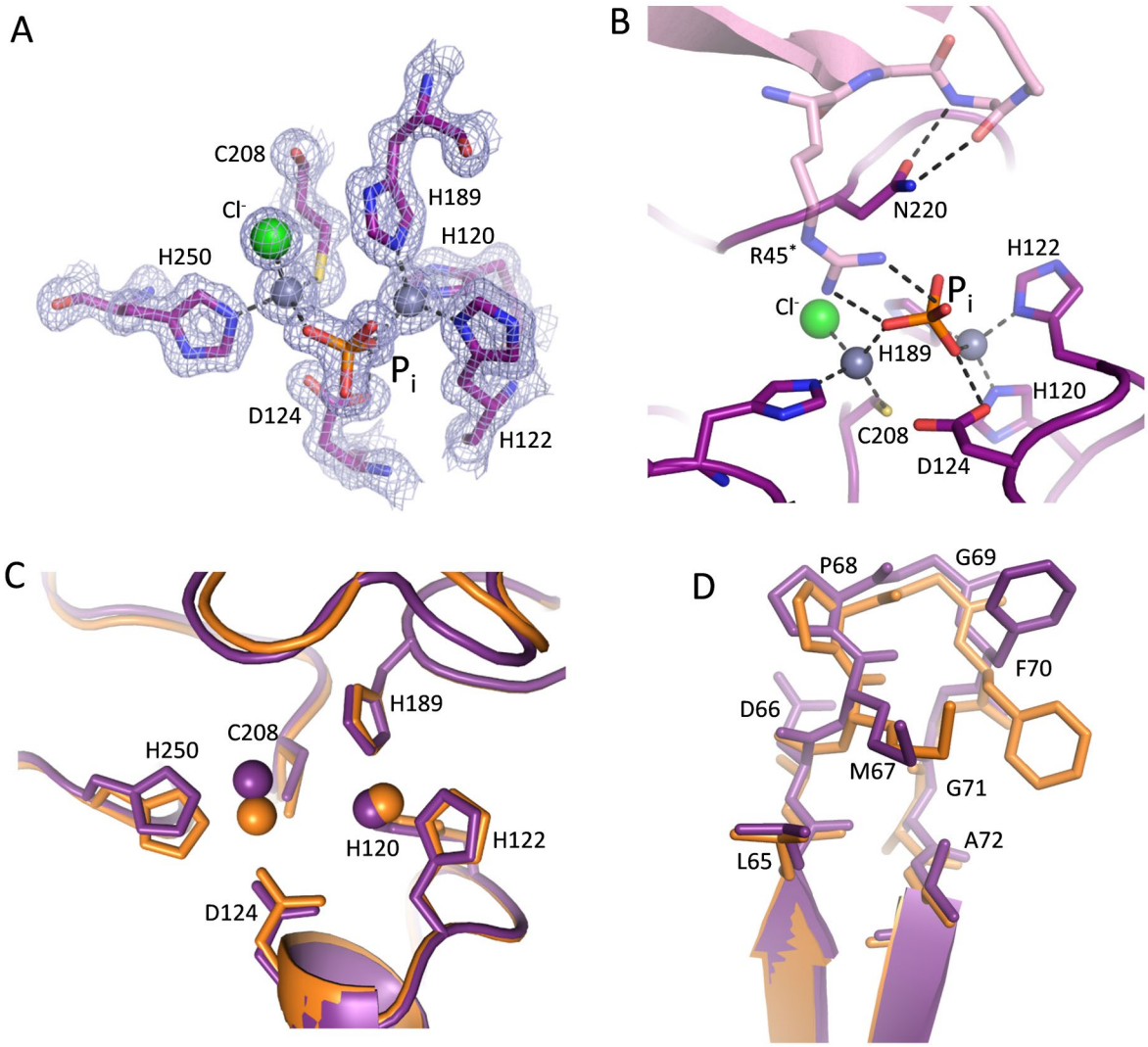

International Journal of Biological Macromolecules

Joanna Raczynska et al.

Figure 6.

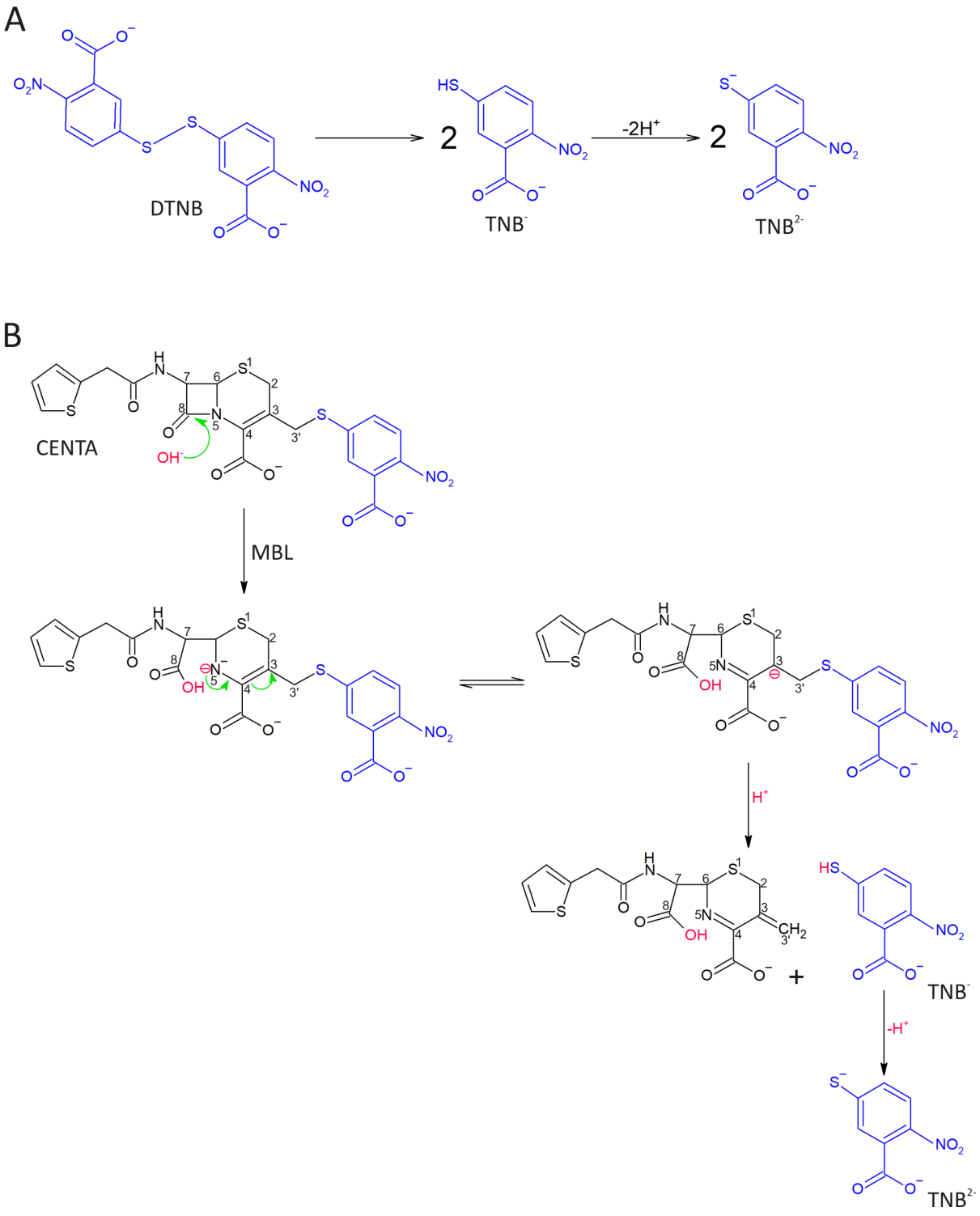

International Journal of Biological Macromolecules

Joanna Raczynska et al.

Figure 7.

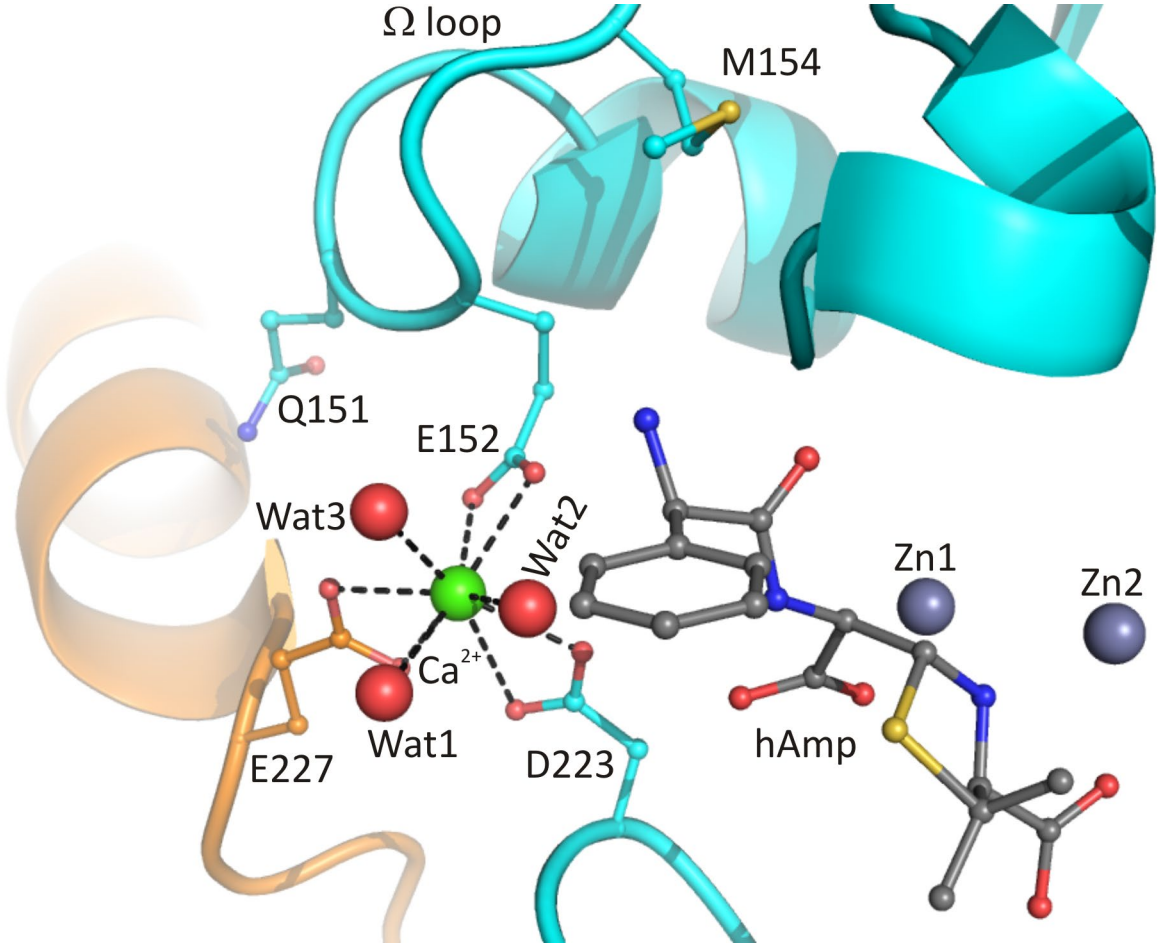

International Journal of Biological Macromolecules

Joanna Raczynska et al.

Figure 8.